Nitromethyl Radical, Cation, and Anion. A Neutralization and Electron Photodetachment−Reionization Mass Spectrometric and ab Initio Computational Study of $[C,H_2,N,O_2]$ Isomers

Miroslav Polášek and František Tureček*

Department of Chemistry, Bagley Hall, University of Washington, Box 351700, Seattle, Washington 98195-1700

Received: August 2, 2000; In Final Form: December 7, 2000

Nitromethyl radical (**1**) was generated in the gas phase by collisional electron detachment from the stable anion $CH_2NO_2^-$ ($\mathbf{1}^-$) and characterized by neutralization−reionization mass spectrometry. Radical **1** was stable on the 3.7 μs time scale. Laser electron photodetachment was also used to generate **1** and probe it by collisional reionization and mass spectrometry in a new experiment denoted as $^-PR^+MS$. The heat of formation of **1** was obtained by G2(MP2) and G2 calculations of enthalpies of atomization, isodesmic, and dissociation reactions as 126 kJ mol^{-1}, in excellent agreement with the value from CCSD(T)/aug-cc-pVTZ calculations, $\Delta H^\circ_{f,298}(\mathbf{1}) = 127$ kJ mol^{-1}. The dissociation energy of the C−H bond in nitromethane was calculated as 425 kJ mol^{-1}. No stable structure was found for singlet cation $\mathbf{1}^+$ in accord with complete dissociation of vertically ionized $\mathbf{1}^+$. Several anionic, radical, and cationic isomers of the general formula $[C,H_2,N,O_2]$ were identified by ab initio calculations and investigated experimentally. $CH_2ONO^\bullet$ (**2**) was generated transiently from the stable cation $\mathbf{2}^+$ and found to dissociate completely to CH_2O and NO on the 3.7 μs time scale. Radical **2** is bound by only 2 kJ mol^{-1}. Gas-phase deprotonation of methyl nitrite and *N*-hydroxyformamide, and fluoride anion-induced desilylation of $(CH_3)_3SiCH_2ONO$ produced anions with the $O{-}CH{=}N{-}OH^-$ ($\mathbf{4}^-$) and/or $O{=}CH{-}NH{-}O^-$ ($\mathbf{5}^-$) structures that were used to generate stable radicals **4** and/or **5**. Collisional neutralization of stable $O{=}C{-}NH{-}OH^+$ ($\mathbf{6}^+$) formed transiently radical **6** that dissociated exothermically to CO and $HNOH^\bullet$. Cations $\mathbf{4}^+$ and $\mathbf{6}^+$ were found to partially interconvert following collisional ionization of radicals **4** and **6**.

Introduction

Transient alkyl radicals bearing functional groups have been of interest to both experimentalists[1] and computational chemists.[2] In particular, the nitromethyl radical (**1**) has been considered as a transient intermediate in gas-phase reactions in flames resulting from hydrogen atom abstraction from nitromethane.[3] The stable nitromethyl anion ($\mathbf{1}^-$)[4] was used by Neumark and co-workers to generate nitromethyl radicals by electron photodetachment and measure the electron affinity of **1** by photoelectron spectroscopy.[5] In addition, laser photofragmenation of **1** was studied by the same group and some of the products have been identified following momentum selection.[6] Isomeric radicals of the $[C,H_2,N,O_2]$ family are possible intermediates in reactions of nitrogen oxides with organic molecules, although the structures and stabilities of such elusive intermediates have not been established.

Neutralization−reionization mass spectrometry[7] is a method that allows one to generate transient neutral species from stable cationic or anionic precursors. Briefly, a stable ion precursor is generated by the methods of gas-phase ion chemistry and accelerated to a high velocity (typically 100 000−200 000 m s^{-1}).[7b] The fast ions are selected by their mass to charge (m/z) ratios and a ≈1−10% fraction are discharged by glancing collisions with an atomic[7b] or molecular target.[7c] The remaining ions are deflected electrostatically to provide a fast neutral beam. Owing to the short duration of the neutralizing collision (2−5 $\times$ 10^{-15} s), the neutral intermediates are initially formed with the structure of the precursor ion. Following a few microseconds, the surviving neutral intermediates and products of their unimolecular dissociations are ionized by another collision and analyzed by mass spectrometry. The neutral intermediates can be probed by collisional activation,[1c,8] photoexcitation,[9] photoionization,[10] and their dissociation kinetics can be determined by variable-time measurements.[11] In addition, product mass analysis is achieved readily at unit mass resolution following collisional ionization thus allowing for efficient product identification by mass spectrometry. Several elusive molecules and radicals containing NO and NO_2 groups have been generated and characterized previously by NRMS.[12−20]

In the work described here we studied the formation of radical **1** by femtosecond collisional electron transfer. In addition, we report experimental and computational studies of several isomeric radicals of the general formula $[C,H_2,N,O_2]$. We were interested in preparing the radicals unambiguously from stable ion precursors and investigated the radical stabilities and unimolecular dissociations. High-level ab initio calculations were used to provide ion and radical energies to assess the dissociation and isomerization enthalpies in the gas phase.

Experimental Section

Methods. Measurements were made on a tandem quadrupole acceleration−deceleration mass spectrometer described previously.[21] The instrument was equipped with a Coherent-Innova 90 argon ion laser that was operated at 6 W CW power output at the main visible lines (488 and 514.5 nm). Precursor cations

* Corresponding author. Tel: (206) 685-2041. Fax: (206) 685-3478. E-mail: turecek@chem.washington.edu.

10.1021/jp002758a CCC: $20.00
Published on Web 02/02/2001

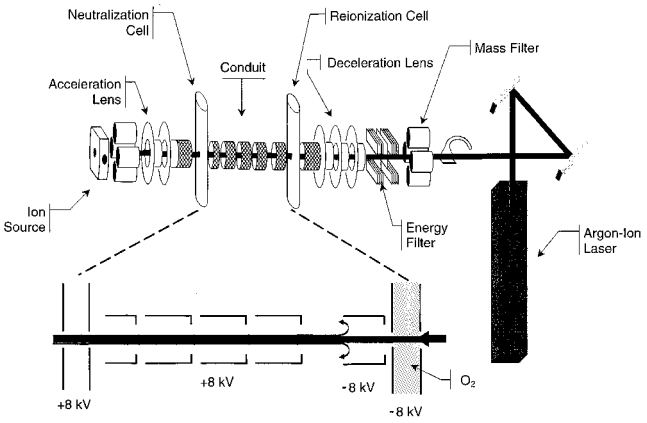

Figure 1. Electrostatic potential settings for laser photodetachment experiments.

were generated by dissociative ionization in an electron ionization (EI) ion source, or by ion−molecule reactions in a tight chemical ionization (CI) ion source. Typical EI source conditions were as follows: emission current 0.5 mA, sample pressure $5-8 \cdot 10^{-6}$ Torr, electron energy 70 eV, temperature 250 °C. Typical CI source conditions were as follows: emission current 1 mA, sample pressure $(1-2) \times 10^{-4}$ Torr as measured at the diffusion pump intake, electron energy 100 eV, and temperature 250−300 °C. Negative ions were generated in the negative CI source (NCI) using a variety of reagent gases as specified below. Typical NCI conditions were as follows: emission current 1 mA, sample pressure $(1-2) \times 10^{-4}$ Torr as measured at the diffusion pump intake, electron energy 200 eV, and temperature 250−300 °C.

Stable ions were extracted form the ion source, accelerated by a potential drop of 8160 V to a high kinetic energy and discharged by collisions in a floated collision cell. For cations, neutralization was achieved by collisions with dimethyl disulfide that was admitted at pressures to achieve 70% transmittance of the precursor ion beam. Poisson distribution predicts that under these conditions >83% of colliding ions undergo single collisions. Anions were discharged by collisions with O_2 at 70% ion transmittance. The radical intermediates and dissociation products were allowed to drift 60 cm to reach a down-beam reionization collision cell in 3.7 μs. Collisional activation of neutral intermediates was achieved by admitting helium in the differentially pumped drift region to allow for 50% or 70% transmittance of the fast beam. Reionization to cations was carried out by collisions with O_2 that was admitted at pressure allowing 70% ion transmittance. Reionization to anions was carried out by collisions with benzene vapor at 70% ion transmittance.

Laser photodetachment experiments were conducted in the drift region in which electrostatic potentials were adjusted as shown in Figure 1. Precursor anions were accelerated to 8240 eV and transmitted to the drift region that was pumped to 10^{-7} Torr. The region was maintained at +8160 V to allow unimpeded transmission of anions, and the ion beam was coaxially irradiated with the light beam from the Ar ion laser. The laser beam had a focal point between the deceleration lens and the quadrupole mass analyzer and overlapped with ca. 40% of the fast anion beam. The precursor anions were stopped by a −8240 V potential applied to the reionization cell, whereas neutral products passed unimpeded. Collisional ionization to cations occurred in the reionization cell, and the ions were decelerated to ca. 80 eV kinetic energy, energy-filtered, and mass analyzed by the quadrupole mass spectrometer. The quadrupole mass filter was floated at ±79 V to achieve unit mass resolution. Several scans with laser on and laser off were acquired and the scans were subtracted to compensate for the contribution of radicals formed by collisional neutralization. The spectra obtained by neutralization of cations followed reionization to cations are denoted by $^{+}NR^{+}$ and represent averages of 30−50 repetitive scans. The spectra obtained by neutralization of anions followed by reionization to cations are denoted by $^{-}NR^{+}$ and represent averages of 50−100 repetitive scans. The spectra obtained by neutralization of anions followed by reionization to anions are denoted by $^{-}NR^{-}$ and represent averages of 500−1000 repetitive scans.

Materials. Nitromethane, nitromethane-d_3, dimethyl disulfide, *N*-hydroxyurethane (all Aldrich), benzene (Fisher), nitrogen trifluoride (Air Products), and nitrous oxide (Matheson) were used as received. Methyl nitrite and ethyl nitrite were prepared according to a literature procedure by dropping 20% sulfuric acid to stoichiometric mixtures of methanol and ethanol, respectively, and sodium nitrite at 0 °C.[22] The escaping gaseous nitrites were passed through a solution of sodium hydroxide, dried with solid calcium chloride, and trapped at −78 °C. The nitrites were stored at −20 °C in 1 L glass ampules that were wrapped in aluminum foil to prevent photolysis, and trap-to-trap redistilled before use. Trimethylsilylmethyl nitrite was prepared analogously by nitrosation of trimethylsilylmethanol (Aldrich), dried, and purified by trap-to-trap distillation. Mass spectrum (*m*/*z*, relative intensity): 133 ($M^{\bullet+}$, absent), 118 (0.4), 88 (13), 75 (12), 74 (9), 73 (100), 61 (4), 60 (2), 59 (7), 58 (13), 57 (2), 55 (2), 45 (24), 44 (4), 43 (13), 42 (3), 30 (4), 29 (4). *N*-Hydroxyformamide was prepared from hydroxylamine and ethyl formate according to a literature procedure.[23] Mass spectrum (*m*/*z*, relative intensity): 61 ($M^{\bullet+}$, 70), 45 (2), 44 (6), 43 (25), 42 (5), 33 (100), 32 (41), 31 (6), 30 (11), 29 (69), 28 (98), 27 (6), 26 (1), 17 (6), 16 (11), 15 (2).

Calculations. Standard ab initio calculations were performed using the Gaussian 98 suite of programs.[24] Geometries were optimized at two levels of theory. Density functional calculations[25] employed Becke's hybrid functional (B3LYP)[26] and the 6-31+G(d,p) or 6-311+G(2df,p) basis sets. In addition, all structures were reoptimized using the 6-31+G(d,p) basis set with perturbational Møller−Plesset calculations[27] truncated at second order and employing excitations of all electrons, MP2-(FULL). Comparison of B3LYP and MP2(FULL) optimized geometries was useful for detecting possible cases of pathological behavior of either approximation. Stationary points were characterized by harmonic frequency analysis as local minima (all frequencies real) or first-order saddle points (one imaginary frequency). The B3LYP frequencies were scaled by 0.963[28] (for other scaling factors see refs 29−31). Single-point energies were calculated on both sets of optimized geometries using the composite Gaussian 2 (MP2)[32] scheme that consists of a quadratic configuration interaction calculation, QCISD(T)/6-311G(d,p),[33] and a basis set expansion through MP2/6-311G-(d,p) and MP2/6-311+G(3df,2p) calculations. In addition, coupled-clusters single-point energies[34,35] were calculated with CCSD(T)/6-311G(d,p)[36] and used in the G2(MP2) scheme. A somewhat higher level of theory consisted of Gaussian 2 calculations[37] that used basis set expansion through MP4-(SDTQ)/6-311G(d,p), 6-311+G(d,p) and 6-311G(2df,p) single-point energies, which were combined with the MP2/6-311+G-(3df,2p) and QCISD(T) or CCSD(T) single-point energies as described.[37] Finally, at a yet higher level of theory a few selected systems were treated with CCSD(T) single-point calculations using Dunning's correlation-consistent triple-ζ basis set augmented with diffuse functions on all atoms, aug-cc-pVTZ.[38]

Results and Discussion

Ion Preparation. The generation of transient neutral intermediates by femtosecond collisional electron transfer mandates that the ion precursors be prepared with well-defined structures. The nitro, nitroso, and nitrite groups substantially affect ion stabilities, so that a combined approach utilizing cations or anions is necessary to generate precursors for radical intermediates. Ion structures and relative energies were deduced from ab initio calculations.

A logical precursor for the nitromethyl radical was the stable nitromethyl anion, $CH_2NO_2^-$ (**1**$^-$), which is readily prepared by gas-phase deprotonation of nitromethane.[4] As a gas-phase base we used the fluoride anion that was generated from NF_3 under negative chemical ionization (NCI) conditions and provided excellent yields of ion **1**$^-$.[5] Proton transfer from nitromethane to F^- is 57−64 kJ mol^{-1} exothermic according to the experimental and calculated gas-phase acidities (ΔH_{acid})[39] of nitromethane[40−42] and HF.[43]

In contrast, the CH_2O-NO^- anion (**2**$^-$) apparently does not arise by gas-phase deprotonation of methyl nitrite that was reported to result in isomerization to form $ON-CH_2-O^-$ (**3**$^-$) instead.[4] Our attempts to generate anion **2**$^-$ by desilylation with F^- of $(CH_3)_3Si-CH_2ONO$ (Scheme 2) resulted in an ion that

SCHEME 1

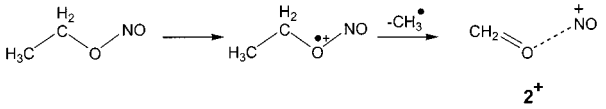

SCHEME 2

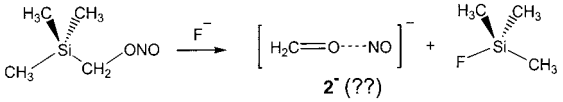

was identical with the product of deprotonation of methyl nitrite, which, however, was not **3**$^-$ but **4**$^-$ and/or **5**$^-$, as discussed below. Interestingly, the NF_3-NCI mass spectrum of $(CH_3)_3Si-CH_2ONO$ was similar to the self-NCI spectrum and both showed a prominent $[C,H_2,N,O_2]^-$ ion at *m*/*z* 60 (Figure 2). The other ions observed in the spectra were the precursor anion radical at *m*/*z* 133, $(CH_3)_3SiO^-$ at *m*/*z* 89, $OCNO^-$ at *m*/*z* 58, and CNO^- at *m*/*z* 42 (Figure 2). However, an ionic precursor of $CH_2ONO^\bullet$ (**2**) was generated by dissociative ionization of ethyl nitrite that provided the CH_2O-NO^+ cation (**2**$^+$) in high yield (Scheme 1)[17] that was used to generate the corresponding transient radical. Deprotonation of *N*-hydroxyformamide with F^- was used to generate anions with the O−N−C−O framework.[4] From the calculated anion relative stabilities and topical gas-phase acidities, deprotonation with F^- was expected to occur exothermically at either N or O to form a mixture of isomeric anions **4**$^-$ and **5**$^-$, eqs 1 and 2.

$$O{=}CH-NH-OH + F^- \rightarrow O-CH{=}N-OH^- + HF \quad (\mathbf{4}^-)$$
$$\Delta H_{r,298} = -122 \text{ kJ mol}^{-1} \quad (1)$$

$$\rightarrow O{=}CH-NH-O^- + HF \quad (\mathbf{5}^-)$$
$$\Delta H_{r,298} = -75.5 \text{ kJ mol}^{-1} \quad (2)$$

Selective deprotonation was attempted using HS^- ($\Delta H_{acid}(H_2S)$ = 1469−1473 kJ mol^{-1})[44] as a gas-phase base that was assumed to react selectively with the N−H bond of ΔH_{acid} = 1433 kJ mol^{-1} to form the more stable **4**$^-$, while the less acidic O−H bond of ΔH_{acid} = 1479 kJ mol^{-1} should be unreactive. However, under H_2S-NCI conditions *N*-hydroxyformamide underwent a variety of ion−molecule reactions that co-formed COS^- and CH_2NS^- that overlapped with **4**$^-$ at *m*/*z* 60 and represented major contaminants.

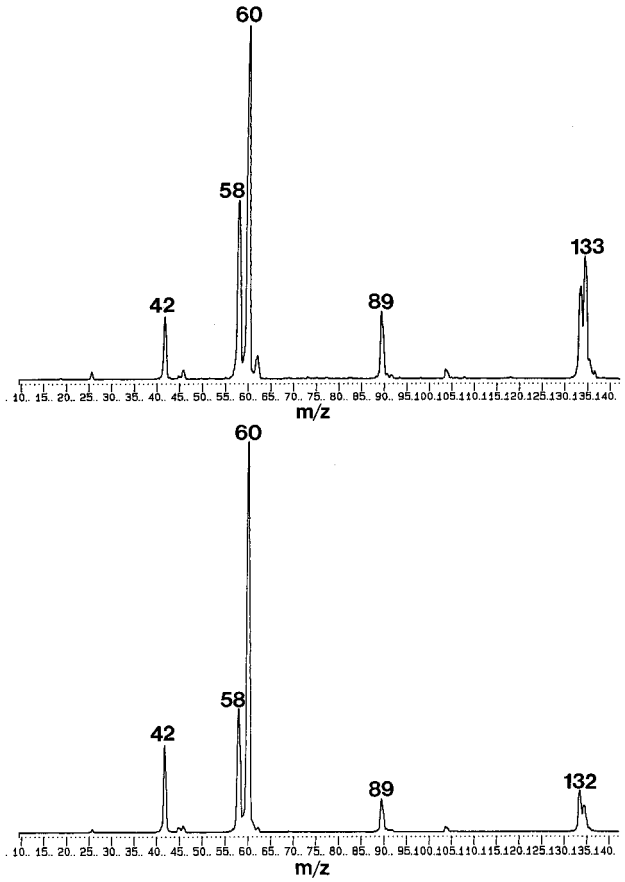

Figure 2. Negative chemical ionization (NCI) mass spectra of $(CH_3)_3SiCH_2ONO$: (top) ionization with NF_3/F^-; (bottom) self-NCI.

A cation isomer with the O−N−C−O bond connectivity (**6**$^+$) was generated by dissociative ionization of ethyl *N*-hydroxycarbamate (Scheme 3). The high-resolution mass spectrum of

SCHEME 3

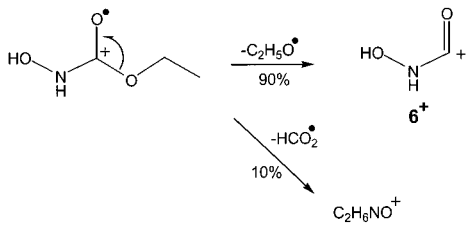

the *m*/*z* 60 cation showed that the loss of the ethoxy radical from ethyl *N*-hydroxycarbamate was accompanied by elimination of an HCO_2 radical that produced a $C_2H_6NO^+$ cation that had the same nominal mass as **6**$^+$ and could not be resolved in NRMS measurements. The [**6**$^+$]/[$C_2H_6NO^+$] abundance ratio from high-resolution measurements was 90/10.

Attempts were also made to generate the most stable carbamate anion **10**$^-$ as a precursor for radical **10**. Gas-phase deprotonation with F^- of carbamic acid, which in turn was produced by vacuum sublimation of ammonium carbamate,

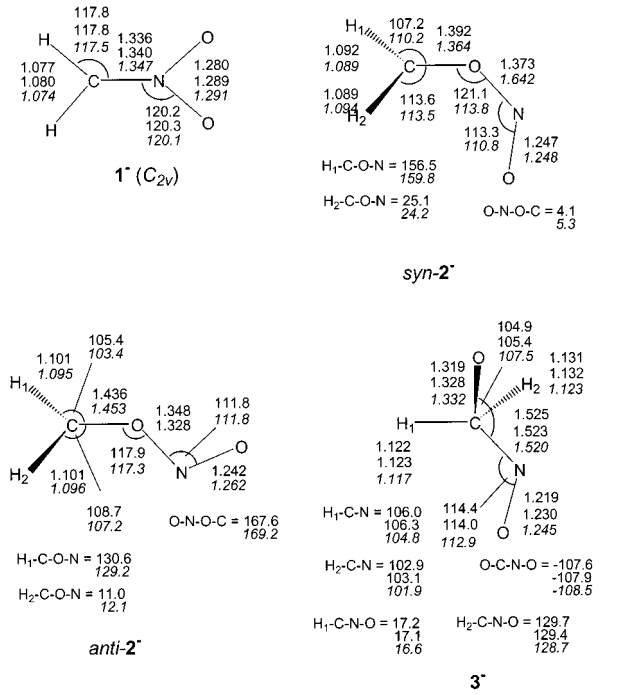

Figure 3. Optimized structures of $\mathbf{1}^-$−$\mathbf{3}^-$. Bond lengths in angstroms, bond and dihedral angles in degrees. Top roman numerals: B3LYP/6-311+G(2df,p) parameters. Bottom roman numerals: B3LYP/6-31+G(d,p) parameters. Italics: MP2(FULL)/6-31+G(d,p) parameters.

formed a weak anion at *m*/*z* 60. Unfortunately, the low intensity of the *m*/*z* 60 ion beam and its instability prevented us from obtaining NR mass spectra. Another attempt on preparation of $\mathbf{10}^-$ was made by gas-phase addition of NH_2^- to CO_2. However, the latter ion−molecule reaction is so exothermic that the intermediate anion $\mathbf{10}^-$ undergoes further isomerization and dissociation to O═C═N$^-$ and H_2O.[45,46]

In summary of ion synthesis, ions with structures $\mathbf{1}^-$, $\mathbf{2}^+$, ($\mathbf{4}^-$ and/or $\mathbf{5}^-$), and $\mathbf{6}^+$ were prepared by ion−molecule reactions or dissociative ionization to be used for collisional neutralization.

Anion Structures and Energetics. Several anions were found by B3LYP and MP2(FULL) calculations to be local minima on the potential energy surface. The optimized structures of $\mathbf{1}^-$−$\mathbf{3}^-$ are summarized in Figure 3. The B3LYP and MP2-(FULL) geometries agreed closely for most anion structures. A notable exception was the structure of *syn*-$\mathbf{2}^-$ for which MP2-(FULL) predicted a substantially longer N−O bond than that from B3LYP calculations. (Figure 3). Interestingly, no substantial difference in the optimized geometries was found for the anti-rotamer *anti*-$\mathbf{2}^-$ (Figure 3). Basis set effects on the optimized geometries were checked for $\mathbf{1}^-$ and $\mathbf{3}^-$ and found to be small as the B3LYP/6-311+G(2df,p) structures resembled closely those from B3LYP/6-31+G(d,p) optimizations (Figure 3). The optimized structures of $\mathbf{4}^-$−$\mathbf{11}^-$ are shown in Figure 4.

The anion relative energies are summarized in Table 1. The carbamate anion $\mathbf{10}^-$ was by far the most stable structure within the $[C,H_2,N,O_2]^-$ family of isomers. Regarding the nitromethyl anion of interest, Table 1 shows that isomerization of $\mathbf{1}^-$ by methylene group migration to one of the oxygen atoms is 157 kJ mol^{-1} endothermic to form *anti*-$\mathbf{2}^-$. In contrast, further N → C migration in *anti*-$\mathbf{2}^-$ is 162 kJ mol^{-1} exothermic to form $\mathbf{3}^-$ which is nearly thermoneutral with $\mathbf{1}^-$. A cyclic intermediate for the isomerizations $\mathbf{1}^-$ → *anti*-$\mathbf{2}^-$ and *anti*-$\mathbf{2}^-$ → $\mathbf{3}^-$ was sought but found to collapse to $\mathbf{3}^-$ by N−O bond dissociation. A transition state for one-step isomerization $\mathbf{1}^-$ → $\mathbf{3}^-$ was also sought by B3LYP and MP2(FULL) calculations. The potential

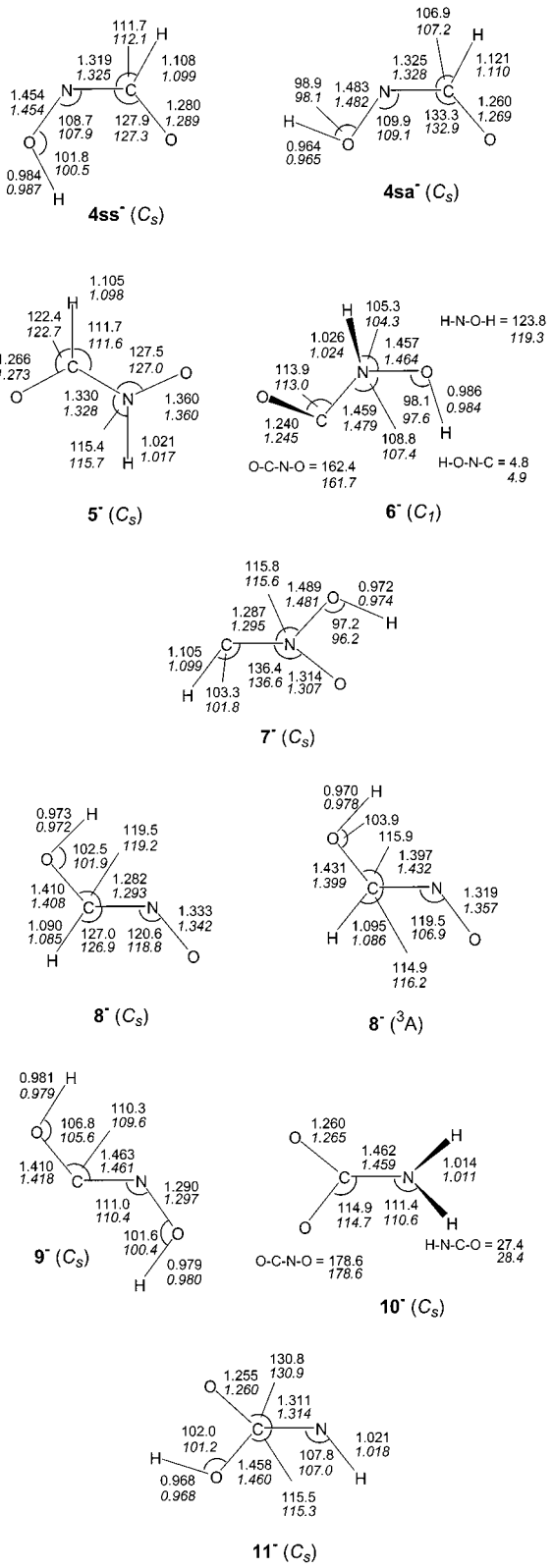

Figure 4. Optimized anion structures. Bond lengths in angstroms, bond and dihedral angles in degrees. Roman numerals: B3LYP/6-31+G-(d,p) parameters. Italics: MP2(FULL)/6-31+G(d,p) parameters.

energy profile showed a 138−144 kJ mol^{-1} increase upon stepwise shortening of the N−O bond distance from 2.3 Å in $\mathbf{3}^-$ to 1.4 Å in 0.1 Å steps. However, frequency analysis at several points along the reaction coordinate showed positive curvature of the potential energy surface which did not converge to a saddle point. This indicated that at the present level of theory, using single-determinant reference wave functions,

TABLE 1: Relative Energies of [C,H$_2$,N,O$_2$] Anions

ion	relative energy[a] B3LYP/ 6-31+G(d,p)	QCISD(T)/[b] 6-311+G(3df,2p)	CCSD(T)/[c] 6-311+G(3df,2p)
$CH_2NO_2^-$ (**1**)	0	0	0
syn-CH_2ONO^- (*syn*-**2**$^-$)	132	132 (128)[d]	134
anti-CH_2ONO^- (*anti*-**2**$^-$)	157	158 (157)[d]	
OCH_2NO^- (**3**$^-$)	9	−4 (−5)[d]	−4
syn-syn-OCH═NOH$^-$ (**4ss**$^-$)	−160	−180 (−180)[d]	−181
syn-anti-OCH═NOH$^-$ (**4sa**$^-$)	−129	−144 (−144)[d]	
O═CHNHO$^-$ (**5**$^-$)	−128	−133 (−133)[d]	
O═CNHOH$^-$ (**6**$^-$)	−8	−25 (−24)[d]	−26
anti-HC═N(OH)O$^-$ (**7**$^-$)	151	135 (136)[d]	
anti-HOCH═NO$^-$ (**8**$^-$)[e]	−52	−65 (−64)[d]	
trans-HOC═NOH$^-$ (**9**$^-$)	2	−21 (−20)[d]	
H_2NCOO^- (**10**$^-$)	−378	−401 (−401)[d]	−402
$HNCOOH^-$ (**11**$^-$)	−317	−343 (−342)[d]	−343

[a] In units of kJ mol^{-1} at 0 K. [b] Effective energies based on MP2(FULL)/6-31+G(d,p) optimized geometries: E[QCISD(T)/6-311+G(3df,2p)] = E[QCISD)T)/6-311G(d,p)] + E[MP2/6-311+G(3df,2p)] − E[MP2/6-311G(d,p)] + ZPVE. [c] Effective energies based on MP2(FULL)/6-31+G(d,p) optimized geometries: E[CCSD(T)/6-311+G(3df,2p)] = E[CCSD(T)/6-311G(d,p)] + E[MP2/6-311+G(3df,2p)] − E[MP2/6-311G(d,p)] + ZPVE. [d] Effective energies based on B3LYP/6-31+G(d,p) optimized geometries. [e] *syn*-HO−CH═N−O$^-$ rearranged spontaneously to **4ss**$^-$ upon attempted geometry optimization.

anions **1**$^-$ and **3**$^-$ are not interconnected on the singlet potential energy surface. Although the potential energy barrier for the isomerization of **1**$^-$ to **3**$^-$ was not obtained, the properties of the potential energy surface indicated a substantial barrier which we estimate at >140 kJ mol^{-1}. A yet another isomerization of **1**$^-$ by hydrogen migration to form the stable ion **11**$^-$ was calculated to be 135 kJ mol^{-1} endothermic and must have included an additional activation barrier because **11**$^-$ was a local energy minimum. Hence, the relative energies of structurally related anion isomers indicated that unimolecular isomerizations of **1**$^-$ required substantial activation energies that could not be acquired by the anions prepared by mild gas-phase deprotonation of nitromethane. This leads to the conclusion that **1**$^-$ prepared from nitromethane was pure.

In contrast, *syn*-**2**$^-$ and *anti*-**2**$^-$ were relatively high-energy structures whose isomerizations to **3**$^-$ were exothermic and could provide sufficient energy to promote further highly exothermic isomerizations by hydrogen atom shifts to form ions **4**$^-$ and **5**$^-$. For example, the overall isomerization *syn*-**2**$^-$ → **4ss**$^-$ was calculated to be 312 kJ mol^{-1} exothermic which is sufficient to drive stepwise isomerizations, e.g., *syn*-**2**$^-$ → **3**$^-$ ($\Delta H_{r,0}$ = −136 kJ mol^{-1}), **3**$^-$ → **8**$^-$ ($\Delta H_{r,0}$ = −61 kJ mol^{-1}), and **8**$^-$ → **4ss**$^-$ ($\Delta H_{r,0}$ = −115 kJ mol^{-1}). Although the mechanism for such anion rearrangements has not been elucidated here, the $^-$NR$^-$ mass spectra shown and discussed below indicated that anions **4**$^-$ and/or **5**$^-$ were formed upon attempted preparation of **2**$^-$.

It is interesting to note that anions *syn*- and *anti*-**2**$^-$ are metastable with respect to electron detachment, as judged from the calculated negative adiabatic electron affinities (Table 2). However, vertical ionization, of *syn*-**2**$^-$ was calculated to require 1.40 eV, while the spin-allowed dissociation to CH_2O and ($^1\Sigma^-$)NO$^-$ was 51 kJ mol^{-1} endothermic. This indicates that *syn*-**2**$^-$ exists in a shallow potential energy well with respect to spontaneous electron detachment, a situation similar to the metastability of $CO_2^{\bullet -}$.[47]

Cation Structures and Energies. Since [C,H$_2$,N,O$_2$]$^+$ cations served as precursors for radicals and appeared as intermediates of collisional reionization in $^-$NR$^+$ and $^+$NR$^+$ spectra, the relevant cation structures and relative energies were also of interest. The optimized structures are given in Figure 5, the relative and dissociation energies are summarized in Table 3. Attempts to locate a potential energy minimum for singlet **1**$^+$ failed. A planar C_{2v} structure was obtained by B3LYP geometry optimizations that was a second-order saddle point, while a twisted C_{2v} structure with perpendicular CH_2 and NO_2 groups was a first-order saddle point for degenerate ring opening in the cyclic cation **13**$^+$ (Scheme 4). A high-energy triplet was found for **1**$^+$ that was a local energy minimum (Figure 5). Ion ($^3B_1$) **1**$^+$ was metastable with respect to highly exothermic, spin-forbidden, dissociation to CH_2O + ($^1\Sigma^+$)NO$^+$ but stable against

TABLE 2: Ionization Energies and Electron Affinities of [C,H$_2$,N,O$_2$] Radicals

radical	energy[a] B3LYP/ 6-31+G(d,p) EA[d]	IE$_a$[e]	QCISD(T)/[b,c] 6-311+G(3df,2p) EA[d]	IE$_a$[e]	IE$_v$[f]
1	2.58		2.40		10.84
2	−0.22	8.40	−0.66	8.23	
3	*g*				
4ss	2.43	12.47	2.40	11.93	
5	1.65	9.85	1.62	9.26	
6	1.32	7.93	1.28	7.54	8.99
7	2.38	9.67	2.39	9.54	
8	1.61		1.63		
9	2.03		2.01		
10	3.11		4.00		
11	2.80		2.79		
13		9.11		8.64	

[a] In units of electronvolt at 0 K. [b] From effective single-point energies using B3LYP/6-31+G(d,p) optimized geometries and ZPVE corrections. [c] G2(MP2) electron affinities and ionization energies are 0.131 eV greater than the effective QCISD(T)/6-311+G(3df,2p) values. [d] Electron affinities. [e] Adiabatic ionization energies. [f] Vertical ionization energies. [g] Radical **3** is unstable.

SCHEME 4

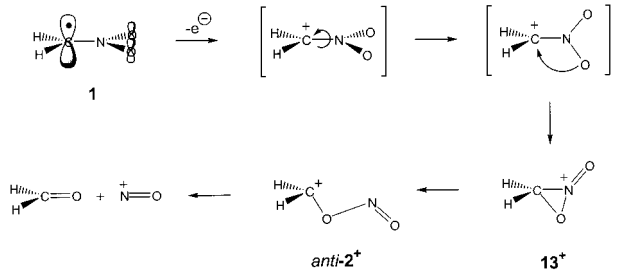

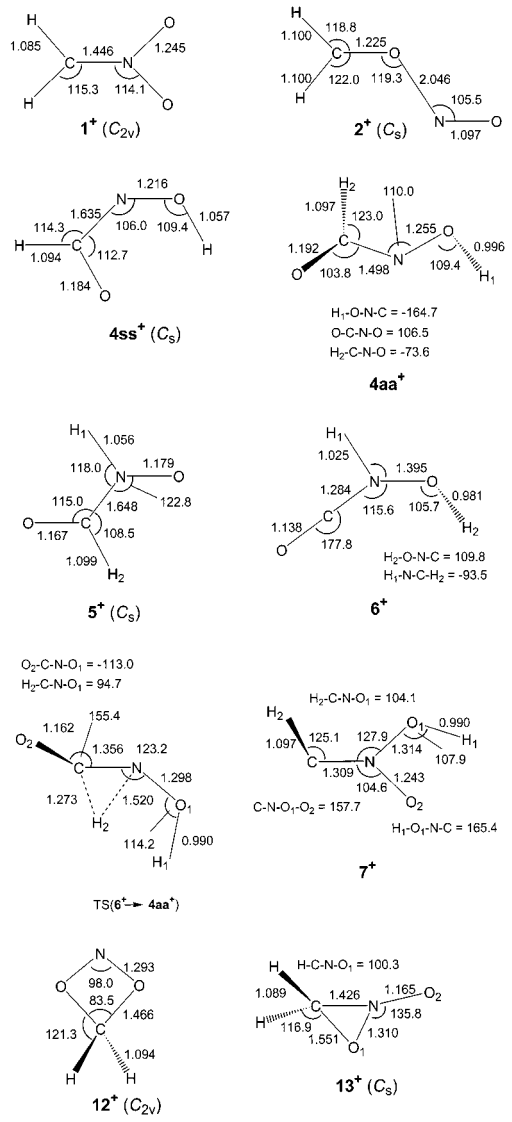

Figure 5. Optimized cation structures. Bond lengths in angstroms, bond and dihedral angles in degrees. Roman numerals: B3LYP/6-31+G(d,p) parameters. Italics: MP2(FULL)/6-31+G(d,p) parameters.

an endothermic, spin-allowed dissociation to $CH_2O + (^3\Sigma^-)NO^+$ (Table 3). Formation of singlet $\mathbf{1}^+$ by vertical ionization of radical **1** is predicted to result in exothermic ring closure to $\mathbf{13}^+$ followed by dissociation of hot $\mathbf{13}^+$ to CH_2O and NO^+. Overall, the dissociation $\mathbf{1}^+ \rightarrow CH_2O + NO^+$ was calculated to be 325 kJ mol^{-1} exothermic (Table 2).

The cyclic cations $\mathbf{12}^+$ and $\mathbf{13}^+$ (Figure 5) can be viewed as topomeric cycloadducts of CH_2O to NO^+. Interestingly, the head-to-tail [2+2] adduct $\mathbf{12}^+$ was somewhat more stable than the head-to-head adduct $\mathbf{13}^+$, although both represented relatively high-energy species that were metastable with respect to cycloreversion (Table 3). The different stabilities of $\mathbf{12}^+$ and $\mathbf{13}^+$ are probably due to bond polarities that favor addition of the negatively charged oxygen atom in CH_2=O to the positively charged nitrogen atom in NO^+.

A ring opening in $\mathbf{12}^+$ and $\mathbf{13}^+$ was calculated to be substantially exothermic to yield cation $\mathbf{2}^+$. The latter structure was bound with respect to dissociation to CH_2=O + NO^+ which required 95 kJ mol^{-1} at 298 K (Table 3). Hence, when formed by dissociative ionization of ethyl nitrite (vide supra), ion $\mathbf{2}^+$ should be stable and not isomerize to cyclic structures.

The most stable cation structure having the nitro group was ion $\mathbf{7}^+$ (Figure 5, Table 3). Dissociation of $\mathbf{7}^+$ to hydrogen cyanate and a hydroxy radical was mildly endothermic requiring 52 kJ mol^{-1} at 298 K. However, Franck−Condon effects in vertical ionization of radical **7** resulted in cation $\mathbf{7}^+$ acquiring 127 kJ mol^{-1} which was sufficient for dissociation. Two-electron oxidation of $\mathbf{7}^-$ resulted in a yet higher Franck−Condon energy being deposited in $\mathbf{7}^+$ (228 kJ mol^{-1}, Table 3). Therefore, ion $\mathbf{7}^+$ is predicted to dissociate when formed by vertical electron transfer.

Four cations with the O−C−N−O framework were found to be local energy minima, e.g., $\mathbf{4ss}^+$, $\mathbf{4aa}^+$, $\mathbf{5}^+$, and $\mathbf{6}^+$, that differed in the positions of the hydrogen atoms (Figure 5). While $\mathbf{6}^+$ was the most stable cation among those studied, isomerization to $\mathbf{6}^+$ by hydrogen migration in the less stable isomer $\mathbf{4aa}^+$ required a 93 kJ mol^{-1} potential energy barrier, so that the less stable ion should exist as an isolable species in the gas phase. When formed by vertical ionization of radical **4ss**, ion $\mathbf{4ss}^+$ was calculated to acquire ca. 60 kJ mol^{-1} internal energy through Franck−Condon effects. Hence this excitation alone should not be sufficient to drive isomerization to ion $\mathbf{6}^+$. However, two-electron transfer, $\mathbf{4ss}^- \rightarrow \mathbf{4ss} \rightarrow \mathbf{4ss}^+$, was calculated to result in large Franck−Condon effects (171 kJ mol^{-1}), so that the vibrational energy in thus formed $\mathbf{4ss}^+$ was sufficient to drive isomerization to $\mathbf{6}^+$. Note that the isomerization barrier for $\mathbf{4ss}^+ \rightarrow \mathbf{6}^+$ is 112 kJ mol^{-1} above the energy threshold for dissociation to CO and HN−OH^+ (Table 3), so that ion $\mathbf{4ss}^+$ undergoing isomerization will dissociate rapidly.

TABLE 3: Relative and Dissociation Energies of $[C,H_2,N,O_2]^+$ Cations

	relative energy[a]	
cation	B3LYP/ 6-31+G(d,p)	QCISD(T)/[b] 6-311+G(3df,2p)
$\mathbf{1}^+$ ($^3B_1$)	502	534
$\mathbf{2}^+$	39	33
$\mathbf{4ss}^+$	170	157
$\mathbf{4aa}^+$	176	179
$\mathbf{5}^+$	96	89
$\mathbf{6}^+$	0	0
TS($\mathbf{6}^+ \rightarrow \mathbf{4aa}^+$)	266	272
$\mathbf{7}^+$	458	460
$\mathbf{12}^+$	233	223
$\mathbf{13}^+$	285	278
Franck−Condon Energy[c]		
$\mathbf{4ss} \rightarrow \mathbf{4ss}^+$		61
$\mathbf{4ss}^- \rightarrow \mathbf{4ss}^+$		171
$\mathbf{5} \rightarrow \mathbf{5}^+$		57
$\mathbf{6} \rightarrow \mathbf{6}^+$		143
$\mathbf{7} \rightarrow \mathbf{7}^+$		127
$\mathbf{7}^- \rightarrow \mathbf{7}^+$		228
Dissociation Energy[d]		
$\mathbf{2}^+ \rightarrow CH_2$=O + NO^+	144	93 (95)[e]
$\mathbf{1}^+$ (VI)[f] → CH_2=O + NO^+		−325
$\mathbf{1}^+$ (VI)[f] → $\mathbf{13}^+$		−173
$\mathbf{7}^+ \rightarrow HC{=}N{=}O^{+\bullet} + OH^\bullet$	19	45 (52)[e]
$\mathbf{12}^+ \rightarrow CH_2$=O + NO^+	−50	−97 (−89)[e]
$\mathbf{13}^+ \rightarrow CH_2$=O + NO^+	−102	−152 (−145)[e]
$\mathbf{1}^+$ ($^3B_1$) → CH_2=O + ($^1\Sigma^+$)NO^+	−319	−408
$\mathbf{1}^+$ ($^3B_1$) → CH_2=O + ($^3\Sigma$)NO^+	356	306
$\mathbf{6}^+ \rightarrow$ CO + $HNOH^+$	179	153 (157)[e]
$\mathbf{6}^+$(VI)[f] → CO + $HNOH^+$		23
$\mathbf{4ss}^+ \rightarrow$ CO + $HNOH^+$	9	−4 (1)[e]
$\mathbf{4ss}^+$ (VI)[f] → CO + $HNOH^+$		−58

[a] In units of kJ mol^{-1}, 0 K values. [b] Effective G2(MP2) enthalpies including B3LYP/6-31+G(d,p) zero-point corrections. [c] Defined as a difference between the single-point energy of the cation at the geometry of the radical or anion and the single-point energy of the cation equilibrium geometry. [d] $H_{0,\text{products}} - H_{0,\text{reactants}}$. [e] 298 K enthalpies. [f] Ion formed by vertical ionization of radical.

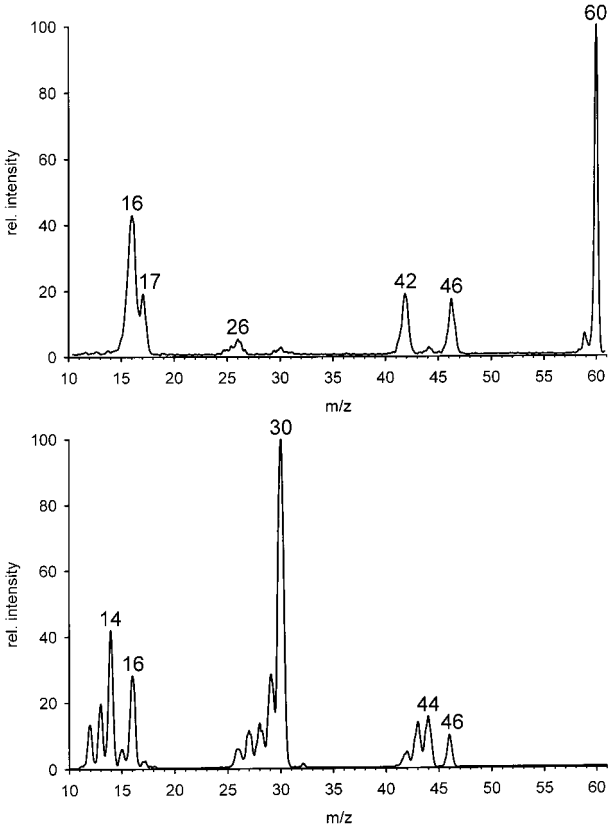

Figure 6. (a, top) $^{-}NR^{-}$ mass spectrum of $CH_2NO_2^-$. (b, bottom) $^{-}NR^{+}$ mass spectrum of $CH_2NO_2^-$.

Radical Formation and Relative Energies. Collisional neutralization of anion $\mathbf{1}^-$ followed by reionization gave rise to $^{-}NR^{-}$ and $^{-}NR^{+}$ spectra shown in Figure 6. The $^{-}NR^{-}$ spectrum showed a prominent survivor ion at *m*/*z* 60 that provided evidence of the kinetic stability of the intermediate radical **1**. The $^{-}NR^{-}$ spectrum further showed peaks of NO_2^- (*m*/*z* 46), NCO^- (*m*/*z* 42), OH^- (*m*/*z* 17), and O^- (*m*/*z* 16), in addition to a few other minor fragments (Figure 6a). The $^{-}NR^{+}$ spectrum of $\mathbf{1}^-$ was dramatically different (Figure 6b). The survivor ion at *m*/*z* 60 was absent, and the spectrum was dominated by the NO^+ peak at *m*/*z* 30. The absence of a survivor cation in the $^{-}NR^{+}$ spectrum is entirely due to the instability of $\mathbf{1}^+$ (vide supra). The major dissociation pathway occurring after reionization consisted of an isomerization of the unstable singlet $\mathbf{1}^+$ by cyclization to form hot $\mathbf{13}^+$ that underwent ring cleavage forming transiently *anti*-$\mathbf{2}^+$, which finally dissociated to CH_2O and NO^+ (Scheme 4). The driving force for the dissociation was provided by the high energy of vertically formed $\mathbf{1}^+$, which was 173 kJ mol^{-1} above $\mathbf{13}^+$, 418 kJ mol^{-1} above $\mathbf{2}^+$, and 325 kJ mol^{-1} above the products. This energy acquired by ionization was evidently sufficient to overcome both the activation barrier for the exothermic isomerization $\mathbf{13}^+ \rightarrow$ *anti*-$\mathbf{2}^+$, and the dissociation energy in the latter ion (Table 3). Interestingly, ($^3B_1$) $\mathbf{1}^+$ was predicted to be bound and its spin-allowed dissociation to CH_2O and ($^3\Sigma^-$)NO was calculated to be 306 kJ mol^{-1} endothermic. The absence of survivor $\mathbf{1}^+$ in the $^{-}NR^{+}$ spectrum indicated that the triplet ion either was not produced by collisional ionization of **1** or underwent fast intersystem crossing followed by highly exothermic dissociation to CH_2O and ($^1\Sigma^+$)NO^+ (Table 3).

Thermochemistry of 1. Since radical **1** is a stable species in the gas phase, its thermochemistry is relevant for evaluating the enthalpies of reactions in which **1** occurs as an intermediate, e.g., hydrogen atom abstraction from nitromethane. The heat of formation of **1** can be inferred from a thermochemical cycle involving proton abstraction from nitromethane and electron detachment from anion $\mathbf{1}^-$ (eq 3). Out of the terms in eq 3, EA(**1**) is known accurately from an electron

$$\Delta H^\circ_{f,298}(\mathbf{1}) = \mathrm{EA}(\mathbf{1}) + \Delta H_{acid}(CH_3NO_2) + \Delta H^\circ_{f,298}(CH_3NO_2) - \Delta H^\circ_{f,298}(H^+) \quad (3)$$

photodetachment measurement (EA = 238.8 kJ mol^{-1}),[5] and the heats of formation of CH_3NO_2 and H^+ are also well-known.[44] However, a large uncertainty in eq 3 originates from the gas-phase acidity of nitromethane which has been reported to range between 1491 and 1498 kJ mol^{-1} with uncertainty limits as large as 9−21 kJ mol^{-1}.[40−42,44] We used the calculated enthalpies of two isodesmic reactions (eqs 4 and 5), dissociation to CH_2O and NO (eq 6), and heats of atomization to evaluate the heat of formation of **1** without involving anion $\mathbf{1}^-$. By comparison, the $\Delta H_{acid}(CH_3NO_2)$ was calculated by G2(MP2)/QCISD(T) as 1498 kJ mol^{-1}. The relevant energies were calculated at the G2(MP2), G2, and CCSD(T)/aug-cc-pVTZ levels of theory, as summarized in Table 4.

$$CH_4 + \mathbf{1} \rightarrow CH_3^\bullet + CH_3NO_2 \quad (4)$$

$$C_2H_6 + \mathbf{1} \rightarrow C_2H_5^\bullet + CH_3NO_2 \quad (5)$$

$$\mathbf{1} \rightarrow CH_2O + NO \quad (6)$$

The calculated $\Delta H^\circ_{f,298}(\mathbf{1})$ showed consistent mean values with scatter within 3.0 kJ mol^{-1} taken as one standard deviation. The mean from the composite G2 and G2(MP2) calculations (126 kJ mol^{-1}) was practically identical with that from the highest-level CCSD(T) calculations (127 kJ mol^{-1}). This suggests $\Delta H^\circ_{f,298}(\mathbf{1}) = 126.5$ kJ mol^{-1} as the best estimate at the present level of theory. When combined with the heat of formation of nitromethane,[44] the C−H bond dissociation energy was calculated as BDE(C−H) = 425 kJ mol^{-1} at 298 K. By comparison, CCSD(T)/aug-cc-pVTZ calculations of the 298 K heat of reaction $CH_3NO_2 \rightarrow \mathbf{1} + H$ gave BDE(C−H) = 421 kJ mol^{-1} while the G2 and G2(MP2) values were 429−430 kJ mol^{-1}. Previously reported values for BDE(C−H) were 450 kJ mol^{-1} from experiment[48] and 384 kJ mol^{-1} from MP2/6-31G-(d,) calculations.[49]

Hydrogen atom abstraction in CH_3NO_2 by OH radical (eq 7) was studied previously by Lin and co-workers,[3f] and so the reaction thermochemistry was also of interest. Our calculations indicate that reaction 7 is 68 kJ mol^{-1} exothermic. The reaction enthalpy that was based on the experimental heats of formation of nitromethane, water, OH radical, and the calculated

$$CH_3NO_2 + OH \rightarrow \mathbf{1} + H_2O \quad (7)$$

$$\Delta H_{rxn,0} = -69 \text{ kJ mol}^{-1}$$

$$\Delta H_{rxn,298} = -68 \text{ kJ mol}^{-1}$$

$\Delta H^\circ_{f,298}(\mathbf{1})$ was $\Delta H_{rxn,298} = -74$ kJ mol^{-1}. Both enthalpies are in very reasonable agreement with the previous value (−74 kJ mol^{-1}) that was obtained at an unspecified level of theory.[3f]

Direct dissociations of **1** by loss of (^{3}P)O atom to form CH_2-NO[50] and by loss of H atom to form triplet nitrocarbene[51] were both substantially endothermic (Table 6). The exothermic dissociation to CH_2O and NO requires a skeletal rearrangement, e.g., endothermic cyclization to **13** followed by exothermic ring

TABLE 4: Heat of Formation of 1

reaction	method	$\Delta H°_{rxn,298}$	$\Delta H°_{f,298}$ (**1**)
1 → (^{3}P)C + 2(^{2}S)H + (^{4}S)N + (^{3}P)O	G2(PMP2)/QCISD(T)	2000.2	123.5
	G2(PMP2)/CCSD(T)	1996	127.7
	G2/QCISD(T)	1999.3	124.5
	G2/CCSD(T)	1995.1	128.6
CH_4 + **1** → $CH_3^•$ + CH_3NO_2	G2(PMP2)/QCISD(T)	−14.0	125.8
	G2(PMP2)/CCSD(T)	−14.0	125.8
	G2/QCISD(T)	−13.8	125.9
	G2/CCSD(T)	−13.8	125.9
	CCSD(T)/aug-cc-pVTZ	−13.3	126.5
C_2H_6 + **1** → $C_2H_5^•$ + CH_3NO_2	G2(PMP2)/QCISD(T)	−0.3	123.4
	G2(PMP2)/CCSD(T)	0.2	123.9
	G2/QCISD(T)	−0.4	123.3
	G2/CCSD(T)	0.1	123.8
1 → CH_2O + NO	G2(PMP2)/QCISD(T)	−155.5	129.9
	G2(PMP2)/CCSD(T)	−155.6	130.0
	G2/QCISD(T)	−155.0	129.4
	G2/CCSD(T)	−155.1	129.5
	CCSD(T)/aug-cc-pVTZ	−152.3	126.7
mean $\Delta H°_{f,298}$(**1**)	G2(PMP2)/QCISD(T)		126 ± 3.0
	G2(PMP2)/CCSD(T)		127 ± 2.6
	G2/QCISD(T)		126 ± 2.6
	G2/CCSD(T)		127 ± 2.6
	CCSD(T)/aug-cc-pVTZ		127
	best value		127

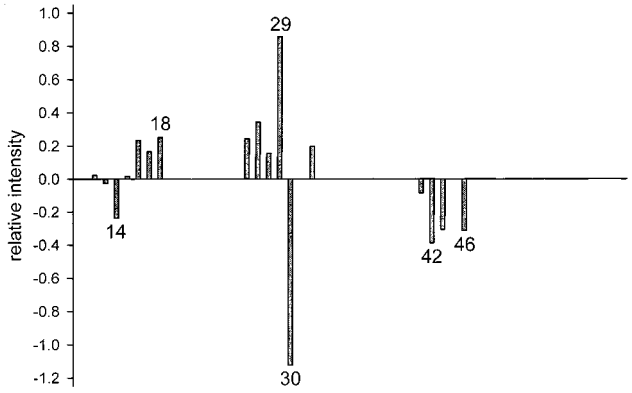

Figure 7. Photodetachment (488 nm)/reionization (O_2, 70% transmittance) mass spectrum of $\mathbf{1}^-$. Positive peaks indicate enhanced ion currents upon laser irradiation.

opening, which are likely to overcome activation energy barriers. Attempts to locate with B3LYP and UMP2(FULL) calculations the transition state for the ring closure **1** → **13** were unsuccessful and led to cusps on the potential energy surface. A multiconfigurational approach appears necessary to map the potential energy surface for the cyclization.

Electron Photodetachment from $\mathbf{1}^-$. The electron affinity of **1** (2.475 eV)[5] makes the anion a suitable target for electron photodetachment using the blue line of an Ar ion laser at 488 nm (2.54 eV). Laser electron photodetachment in $\mathbf{1}^-$ was combined with collisional ionization of the radicals formed to cations; these experiments are denoted as $^-$PR$^+$MS. The $^-$PR$^+$MS of $\mathbf{1}^-$, corrected for background from collisional electron detachment, is presented in Figure 7. Positive peaks in Figure 7 indicate an increase in the reionized ion intensity upon laser irradiation, while negative peaks indicate a decrease. The spectrum shows a decrease of the relative intensities of NO_2^+ (*m*/*z* 46, minor), NCO^+ (*m*/*z* 42, minor), NO^+ (*m*/*z* 30, major), and an increase of the peaks of CHO^+ (*m*/*z* 29, major) and O^+ (*m*/*z* 16, minor). Interpretation of the $^-$PR$^+$ spectra is complicated by cation dissociations following collisional ionization, while collisional ionization by electron capture to form stable anion $\mathbf{1}^-$ was much less efficient than ionization to cations and could not be used in combination with laser electron photodetachment. The difference between the $^-$NR$^+$ and $^-$PR$^+$ spectra probably reflects different internal energy distributions in **1** formed by collisional and photoinduced electron detachment. The presumably less energetic radicals **1** produced by nearly resonant photodetachment do not have enough internal energy

TABLE 5: Radical Relative Energies

	relative energy[a]					
radical	B3LYP/ 6-31+G(d,p)	G2(MP2)/[b] QCISD(T)		G2/[b] QCISD(T)	G2(MP2)/[c] CCSD(T)	G2/[c] CCSD(T)
1	0	0	0[d]	0	0	0
syn-**2**	−137	−164	−166		−164	
4ss	−174	−177	−179	−177	−176	−176
4sa	−159	−156	−160		−156	
5	−217	−209	−209	−209	−209	−209
6	−129		−132			
anti-**7**	133	136	136	135	139	138
syn-**7**	138	144	145	142	146	144
8	−145		−138			
9	−49	−55	−57			
10	−326	−241	−245	−243	−241	−243
11	−294	−305	−305	−306	−305	−306
13	42	44	40	46	46	47

[a] In units of kJ mol^{-1} at 0 K. [b] Relative energies using QCISD(T)/6-311G(d,p) single-point calculations. [c] Relative energies using CCSD(T)/6-311G(d,p) single-point calculations. [d] From single-point energies on B3LYP/6-31+G(d,p) optimized geometries.

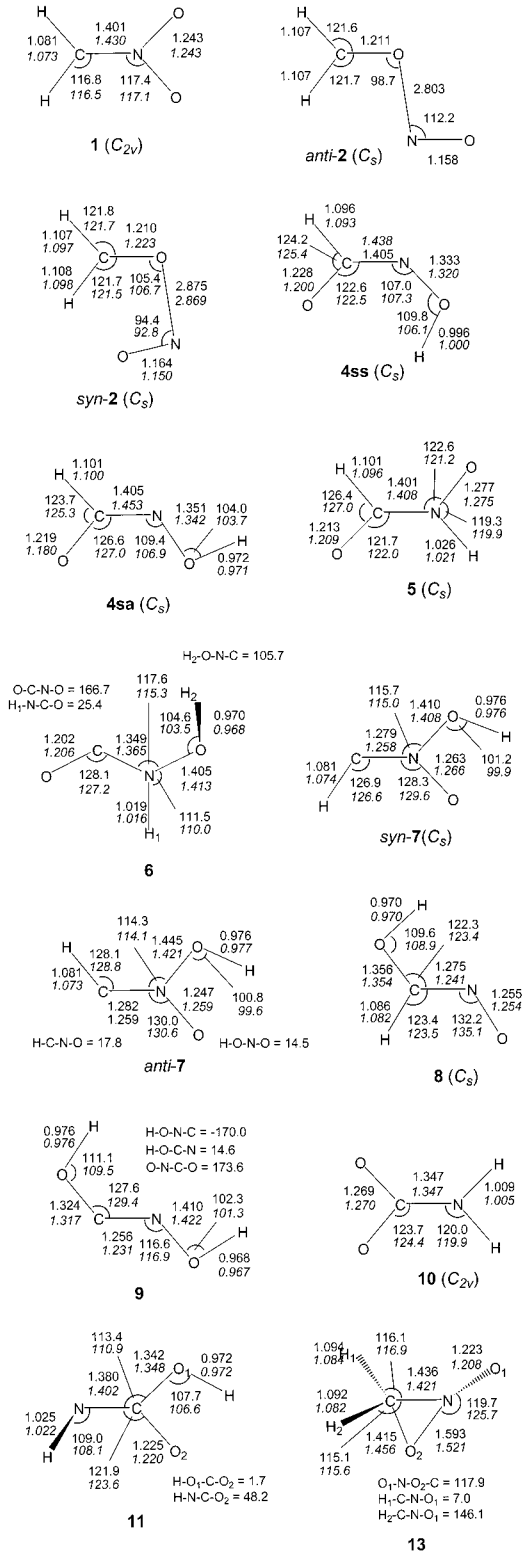

Figure 8. Optimized radical structures. Bond lengths in angstroms, bond and dihedral angles in degrees. Roman numerals: B3LYP/6-31+G(d,p) parameters. Italics: MP2(FULL)/6-31+G(d,p) parameters.

to dissociate which explains the decrease of the NO^+ intensity. The increase of the CHO^+ intensity is due to cation dissociations following collisional reionization and its relation to electron photodetachment is therefore less clear.

[C,H$_2$,N,O$_2$] Isomers. Several structures were obtained for [C,H_2,N,O_2] radicals that were local energy minima as characterized by harmonic frequency analysis. The optimized radical structures are summarized in Figure 8, the relative energies are given in Table 5. Attempts were made to prepare [C,H_2,N,O_2] radicals for which there were ionic precursors and which were relevant to the chemistry of **1**.

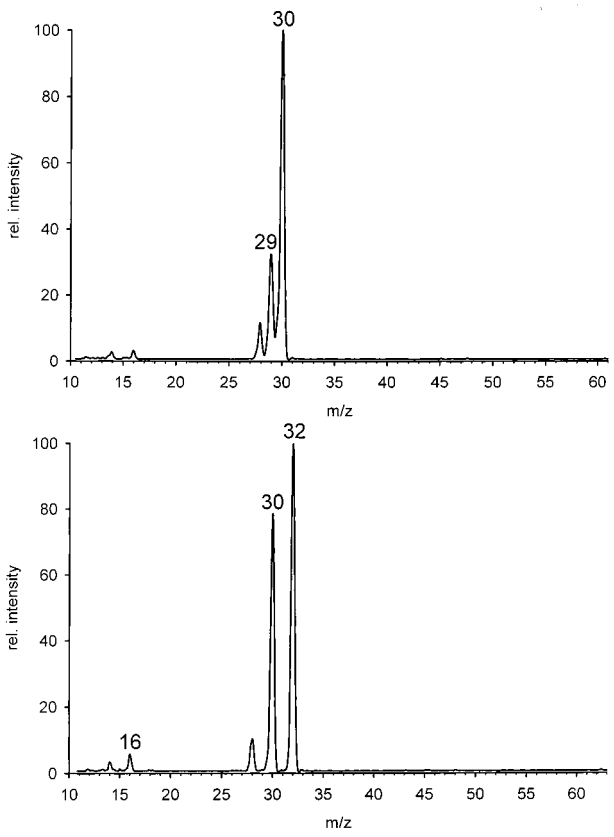

Figure 9. $^+NR^+$ mass spectra of (a, top) CH_2ONO^+, (b, bottom) CD_2ONO^+.

Radical **2** has a stable cationic counterpart (**2**$^+$, Table 3) so that the $^+NR^+$ spectrum can be used to estimate the radical stability with less destructive interference from ion dissociations. The $^+NR^+$ spectrum of **2**$^+$ showed complete dissociation to CH_2O and NO (Figure 9a). These nominally isobaric fragments were distinguished by deuterium labeling that shifted the mass of CD_2O to *m*/*z* 32 and proved that both CD_2O and NO were produced (Figure 9b). The instability of radical **2** was predicted by calculations that indicated very weak bonding in $CH_2O\cdots NO$ (2 kJ mol^{-1}, Table 6) that can be readily overcome by the thermal content of the precursor ion or Franck−Condon energy (E_{FC}) acquired upon vertical neutralization. Indeed, the calculated E_{FC} = 68 kJ mol^{-1} (Table 6) alone was sufficient to drive a fast dissociation of vertically formed **2**.

Radical **3** was expected to be formed from the corresponding anion **3**$^-$ which was postulated by Thomas et al. to be produced by negative chemical ionization of methyl nitrite.[4] The $^-NR^+$ spectrum of **3**$^-$ showed no survivor cation (Figure 10a). In contrast, the $^-NR^-$ spectrum clearly indicated a stable radical intermediate that gave rise to an abundant survivor anion (Figure 10a, inset). An interesting feature of the $^-NR^+$ spectrum was the presence of a fragment at *m*/*z* 32. The latter was identified as $[N,H_2,O]^+$ (HN=OH$^+$ or the more stable $H_2N{=}O^+$)[52] by a mass shift to *m*/*z* 34 $[N,D_2,O^+]$ when the precursor anion was generated from CD_3ONO (Figure 10b). $^-NR^+$ and $^-NR^-$ spectra that were very similar to those of the above anion of presumed structure **3**$^-$ were also obtained for the *m*/*z* 60 anions produced from $(CH_3)_3SiCH_2ONO$ (Figure 11a) and, somewhat unexpectedly, HO−NH−CH=O (Figure 11b). In sharp contrast to the

TABLE 6: Radical Dissociation Energies

reaction	energy[a] B3LYP/ 6-31+G(d,p)	energy[a] QCISD(T)/[b] 6-311+G(3df,2p)
1 → $CH_2NO^{\bullet}$ + (^{3}P)O	250	262
1 → (^{3}A) $HCNO_2$ + H$^{\bullet}$	465	464
2 → CH_2O + NO$^{\bullet}$	0	2
2 (VN)[c] → CH_2O + NO$^{\bullet}$		−65
3 (VN)[d] → CH_2O + NO$^{\bullet}$		−201
4ss → O═CHN═O + H$^{\bullet}$	293	258 (259)[e]
4ss → O═C═NOH + H$^{\bullet}$	211	188 (187)[e]
5 → HC═O$^{\bullet}$ + HN═O	244	232
5 → O═CHN═O + H$^{\bullet}$	339	292 (292)[e]
6 → CO + HNOH$^{\bullet}$	−2	−27
6 (VN) → CO + HNOH$^{\bullet}$		−137
6 → HN═C═O + OH$^{\bullet}$	205	200
8 → HC═NO + + OH$^{\bullet}$	222	207
10 → CO_2 + $NH_2^{\bullet}$	7	−105 (−109)[e]
11 → HN═C═O + OH$^{\bullet}$	371	373

[a] In units of kJ mol^{-1} at 0 K. [b] Effective energies using B3LYP/6-31+G(d,p) optimized geometries. [c] Radical produced by vertical electron capture in the cation. [d] Radical produced by vertical electron detachment from the anion. [e] Effective energies using MP2(FULL)/6-31+G(d,p) optimized geometries.

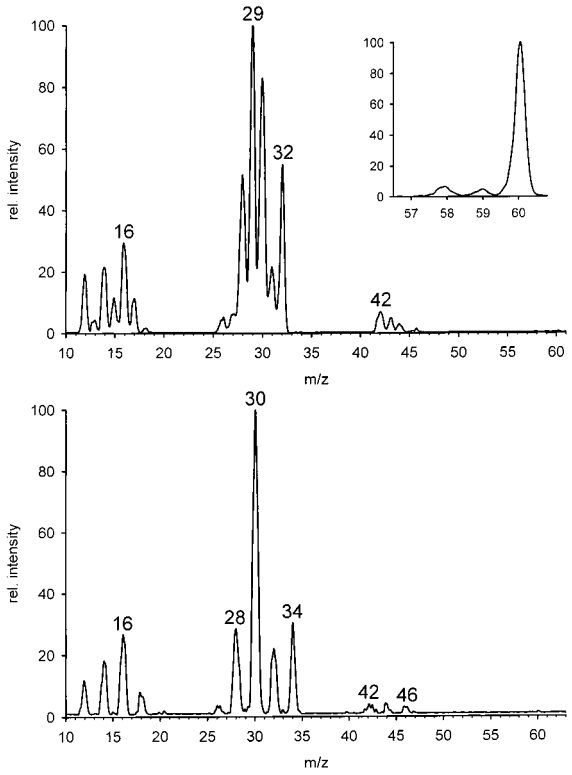

Figure 10. $^-NR^+$ mass spectra of (a, top): $[C,H_2,N,O_2]^-$ from methyl nitrite and (b, bottom): $[C,D_2,N,O_2]^-$ from methyl-d_3 nitrite. Insets show the survivor ion regions in the $^-NR^-$ mass spectra.

experiment, MP2(FULL) and DFT calculations failed to locate an energy minimum for radical **3**, which upon attempted geometry optimizations underwent exothermic dissociation to CH_2O and NO. Moreover, radical **3** formed by vertical electron detachment from **3**$^-$ represented a high-energy point on the repulsive potential energy surface and was expected to dissociate exothermically (Table 6). The intrinsic instability of **3** precludes structure **3**$^-$ for the survivor anion in the $^-NR^-$ spectrum. This result also indicates that the $[C,H_2,N,O]^-$ anion generated from methyl nitrite, $(CH_3)_3SiCH_2ONO$, and HO−NH−CH═O was not **3**$^-$ but a different species, presumably **4**$^-$ (either rotamer) and/or **5**$^-$, formed by anion rearrangement.

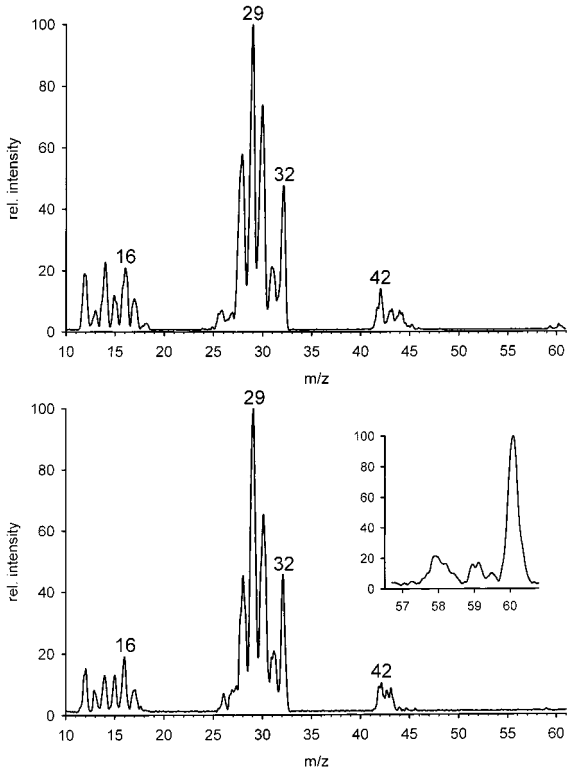

Figure 11. $^-NR^+$ mass spectra of $[C,H_2,N,O_2]^-$ from (a, top) trimethylsilylmethyl nitrite and (b, bottom) *N*-hydroxyformamide. Insets show the survivor ion regions in the $^-NR^-$ mass spectra.

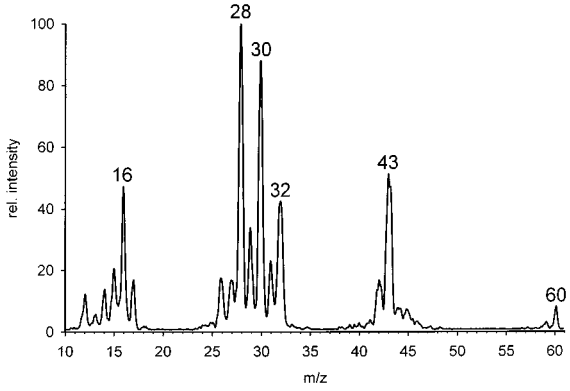

Figure 12. $^+NR^+$ mass spectrum of O═C−NH−OH$^+$ from *N*-hydroxyurethane.

The corresponding radicals **4** (either rotamer) and/or **5** were intrinsically stable, as judged from the optimized geometries (Figure 8) and dissociation energies that were substantially endothermic (Table 6). Hence, electron detachment from **4**$^-$ and/or **5**$^-$ could give rise to nondissociating intermediates, as indicated by the survivor ion in the $^-NR^-$ spectrum. The calculated energies indicated that **4** could rearrange by 1,2-hydrogen atom migration to **6**, and the exothermicity of the isomerization could drive further dissociation to CO and NH−OH. To test this hypothesis, we generated radical **6** by collisional neutralization of the stable cation **6**$^+$ and compared its $^+NR^+$ spectrum with the $^-NR^+$ spectra of **4** and/or **5** (Figure 12). The spectra showed qualitative differences in the relative abundances of several fragments. In particular, loss of OH to form O═C═NH (*m*/*z* 43) and formation of CO (*m*/*z* 28) and HNOH (*m*/*z* 32) were prominent in the spectrum of **6**, consistent with the radical structure, while the *m*/*z* 43 and 28 peaks were weak in the spectra of **4**/**5** which instead showed prominent peaks of CHO^+ at *m*/*z* 29. An attempt was also made to prepare the stable

anion $\mathbf{6}^-$ (Figure 4, Table 1) and compare its $^-NR^+$ spectrum with those of **4** and/or **5**. However, NCI of *N*-hydroxyurethane, a logical precursor of $\mathbf{6}^-$, did not yield an anion at *m*/*z* 60 with an intensity that would be sufficient for a good quality $^-NR^+$ spectrum. Nevertheless, the very different $^+NR^+$ and $^-NR^+$ spectra indicated that radicals **4/5** did not rearrange to large extent to the more stable **6**.

On the basis of the NR spectra and calculated energies, the absence of survivor cations for **4/5** can be assigned to post-reionization dissociations. Table 3 shows that exothermic isomerization of $\mathbf{4aa}^+$ to $\mathbf{6}^+$ requires only a moderate activation barrier ($272-179 = 93$ kJ mol^{-1}) that can be provided by the Franck−Condon energy accompanying the conversion of $\mathbf{4}^-$ to $\mathbf{4}^+$ (171 kJ mol^{-1}). The isomerization forms $\mathbf{6}^+$ with a large excess of vibrational energy that is more than sufficient to drive dissociation to CO + HN−OH$^+$ which is only slightly endothermic (Table 3). Hence, the dissociations of $\mathbf{4}^+/\mathbf{5}^+$ observed upon NR are to a large extent caused by Franck−Condon effects on collisional electron transfer.

Conclusions

The nitromethyl radical **1** is a stable species when formed by collisional electron detachment from anion $\mathbf{1}^-$ in the gas phase. The photodetachment-reionization spectrum of $\mathbf{1}^-$ was different from the $^-NR^+$ spectrum which indicated different internal energy distributions in the intermediate radicals. The chemistry observed on $^-NR^+$ is dominated by cation rearrangements and dissociations following collisional reionization. Several radicals of the [C,H_2,N,O_2] group of isomers were characterized by a combination of positive ion and negative ion neutralization−reionization mass spectra and ab initio calculations.

Acknowledgment. Support of this work by the National Science Foundation (Grant CHE-9712570) is gratefully acknowledged. The computations were performed at the Department of Chemistry Computer Facility that received generous funding from the NSF (Grant CHE-9808182). Dr. Martin Sadilek kindly provided assistance with collisionally activated spectra. We also thank a reviewer for the discussion of anion rearrangements.

References and Notes

(1) (a) Burkey, T. J.; Castelhano, A. L.; Griller, D.; Lossing, F. P. *J. Am. Chem. Soc.* **1983**, *105*, 4701. (b) Hop, C. E. C. A.; Holmes, J. L. *Org. Mass Spectrom.* **1991**, *26*, 476. (c) Shaffer, S. A.; Turecek, F.; Cerny, R. L. *J. Am. Chem. Soc.* **1993**, *115*, 12117. (d) Lazarou, Y. G.; Papagiannakopoulos, P. *J. Phys. Chem.* **1993**, *97*, 9133. (e) Harvey, J. N.; Schroder, D.; Schwarz, H. *Bull. Soc. Chim. Belg.* **1997**, *106*, 447.

(2) (a) MacInnes, I.; Walton, J. C.; Nonhebel, D. C. *J. Chem. Soc., Perkin Trans. 2* **1987**, 1789. (b) Sana M.; Leroy, G.; Peeters, D. *J. Mol. Struct. (THEOCHEM)* **1987**, *36*, 325. (c) Leroy, G.; Sana, M.; Wilante, C. *J. Mol. Struct. (THEOCHEM)* **1991**, *74*, 37. (d) Armstrong, D. A.; Rauk, A.; Yu, D. *J. Am. Chem. Soc.* **1993**, *115*, 666.

(3) (a) Ko, T.; Flaherty, F.; Fontijn, A. *J. Phys. Chem.* **1991**, *95*, 6967. (b) Slemr, F.; Warneck, P. *Ber. Bunsen-Ges. Phys. Chem.* **1975**, *79*, 1163. (c) Salter, L. F.; Thrush, B. A. *J. Chem. Soc., Faraday Trans.* **1977**, *1*, 2025. (d) Nielsen, O. J.; Sidebottom, H. W.; O'Farrell, D. J.; Donlon, M.; Treacy, J. *Chem. Phys. Lett.* **1988**, *146*, 197. (e) Thomsen, E. L.; Nielsen, O. J.; Egsgaard, H. *Chem. Phys. Lett.* **1993**, *215*, 257. (f) Zabarnick, S.; Fleming, J. W.; Lin, M. C. *Chem. Phys.* **1988**, *120*, 319.

(4) Thomas, D. A.; Bloor, J. E.; Bartmess, J. E. *J. Am. Soc. Mass Spectrom.* **1990**, *1*, 295.

(5) Metz, R. B.; Cyr, D. R.; Neumark, D. M. *J. Phys. Chem.* **1991**, *95*, 2900.

(6) Cyr, D. R.; Leahy, D. J.; Osborn, D. L.; Continettin, R. E.; Neumark, D. M. *J. Chem. Phys.* **1993**, *99*, 8751.

(7) For comprehensive reviews of the technique see: (a) Wesdemiotis, C.; McLafferty, F. W. *Chem. Rev.* **1987**, *87*, 485. (b) Holmes, J. L. *Mass Spectrom. Rev.* **1989**, *8*, 513. (c) Turecek, F. *Org. Mass Spectrom.* **1992**, *27*, 1087. (d) Schalley, C. A.; Hornung, G.; Schroder, D.; Schwarz, H. *Chem. Soc. Rev.* **1998**, *27*, 91. (e) Zagorevskii, D. V.; Holmes, J. L. *Mass Spectrom. Rev.* **1999**, *18*, 87.

(8) (a) Danis, P.; Feng, R.; McLafferty, F. W. Anal. *Chem.* **1986**, *58*, 348. (b) Turecek, F.; Drinkwater, D. E.; McLafferty, F. W. *Org. Mass Spectrom.* **1989**, *24*, 669.

(9) (a) Sadilek, M.; Turecek, F. *Chem. Phys. Lett.* **1996**, *263*, 203. (b) Frank, A, J.; Sadilek, M.; Ferrier, J. G.; Turecek, F. *J. Am. Chem. Soc.* **1997**, *119*, 12343.

(10) Sadilek, M.; Turecek, F. *J. Phys. Chem.* **1996**, *100*, 9610.

(11) (a) Kuhns, D. W.; Turecek, F. *Org. Mass* Spectrom. **1994**, *29*, 463. (b) Kuhns, D. W.; Shaffer, S. A.; Tran, T. B.; Turecek, F. *J. Phys. Chem.* **1994**, *98*, 4845.

(12) O'Bannon, P. E.; Sulzle, D.; Dailey, W. P.; Schwarz, H. *J. Am. Chem. Soc.* **1992**, *114*, 344.

(13) Egsgaard, H.; Carlsen, L.; Florencio, H.; Drewello, T.; Schwarz, H. *Ber. Bunsen-Ges. Phys. Chem.* **1989**, *93*, 76.

(14) O'Bannon, P. E.; Sulzle, D.; Schwarz, H. *Helv. Chim. Acta* **1991**, *74*, 2068.

(15) Egsgaard, H.; Carlsen, L.; Florencio, H.; Drewello, T.; Schwarz, H. *Chem. Phys. Lett.* **1992**, *199*, 643.

(16) Polasek, M.; Turecek, F. *J. Phys. Chem. A* **1999**, *103*, 9241.

(17) Polasek, M.; Sadilek, M.; Turecek, F. *Int. J. Mass Spectrom.* **2000**, *196*, 101.

(18) Polasek, M.; Turecek, F. *J. Am. Chem. Soc.* **2000**, *122*, 437.

(19) Polasek, M.; Turecek, F. *J. Am. Soc. Mass Spectrom.* **2000**, *11*, 380.

(20) Polasek, M.; Turecek, F. *J. Am. Chem. Soc.* **2000**, *122*, 9511.

(21) Turecek, F.; Gu, M.; Shaffer, S. A. *J. Am. Soc. Mass Spectrom.* **1992**, *3*, 493.

(22) Gilman, J. P.; Hsieh, T.; Meisels, G. G. *J. Chem. Phys.* **1983**, *78*, 1174.

(23) Fishbein, W. N.; Daly, J.; Streeter, C. L. *Anal. Biochem.* **1969**, *28*, 13−24.

(24) Frisch, M. J.; Trucks, G. W.; Schlegel, H. B.; Scuseria, G. E.; Robb, M. A.; Cheeseman, J. R.; Zakrzewski, V. G.; Montgomery, J. A., Jr.; Stratmann, R. E.; Burant, J. C.; Dapprich, S.; Millam, J. M.; Daniels, A. D.; Kudin, K. N.; Strain, M. C.; Farkas, O.; Tomasi, J.; Barone, V.; Cossi, M.; Cammi, R.; Mennucci, B.; Pomelli, C.; Adamo, C.; Clifford, S.; Ochterski, J.; Petersson, G. A.; Ayala, P. Y.; Cui, Q.; Morokuma, K.; Malick, D. K.; Rabuck, A. D.; Raghavachari, K.; Foresman, J. B.; Cioslowski, J.; Ortiz, J. V.; Stefanov, B. B.; Liu, G.; Liashenko, A.; Piskorz, P.; Komaromi, I.; Gomperts, R.; Martin, R. L.; Fox, D. J.; Keith, T.; Al-Laham, M. A.; Peng, C. Y.; Nanayakkara, A.; Gonzalez, C.; Challacombe, M.; Gill, P. M. W.; Johnson, B.; Chen, W.; Wong, M. W.; Andres, J. L.; Gonzalez, C.; Head-Gordon, M.; Replogle, E. S.; Pople, J. A. *Gaussian 98*, Revision A.6; Gaussian, Inc.: Pittsburgh, PA, 1998.

(25) Parr, R. G.; Yang, W. *Density Functional Theory of Atoms and Molecules*; Oxford University Press: New York, 1989.

(26) (a) Becke, A. D. *J. Chem. Phys*, **1993**, *98*, 1372 and 5648. (b) Stephens, P. J., Devlin, F. J., Chablowski, C. F., Frisch, M. J. *J. Phys. Chem.* **1994**, *98*, 11623.

(27) Møller, C.; Plesset, M. S. *Phys. Rev.* **1934**, *46*, 618.

(28) Rauhut, G.; Pulay, P. *J. Phys. Chem.* **1995**, *99*, 3093.

(29) Finley, J. W.; Stephens, P. J. *J. Mol. Struct. (THEOCHEM)* **1995**, *227*, 357.

(30) Wong, M. W. *Chem. Phys. Lett.* **1996**, *256*, 391.

(31) Scott, A. P.; Radom, L. *J. Phys. Chem.* **1996**, *100*, 16502.

(32) (a) Curtiss, L. A.; Raghavachari, K.; Pople, J. A. *J. Chem. Phys.* **1993**, *98*, 1293. (b) Curtiss, L. A.; Raghavachari, K.; Redfern, P. C.; Pople, J. A. *J. Chem. Phys.* **1997**, *106*, 1063. (c) Raghavachari, K.; Stefanov, B. B.; Curtiss, L. A. *J. Chem. Phys.* **1997**, *106*, 6764.

(33) Pople, J. A.; Head-Gordon, M.; Raghavachari, K. *J. Chem. Phys*, **1987**, *87*, 5968.

(34) Cizek, J. *Adv. Chem. Phys*. **1969**, *14*, 35.

(35) Purvis, G. D.; Bartlett, R. J. *J. Chem. Phys.* **1982**, *76*, 1910.

(36) Curtiss, L. A.; Raghavachari, K.; Pople, J. A. *J. Chem. Phys.* **1995**, *103*, 4192.

(37) Curtiss, L. A.; Raghavachari, K.; Trucks, G. W.; Pople. J. A. *J. Chem. Phys.* **1991**, *94*, 7221.

(38) Dunning, T. H., Jr. *J. Chem. Phys*, **1989**, *90*, 1007.

(39) These are defined as $\Delta H_{acid} = \Delta H_{r,298}$ for the heterolytic bond dissociation HA → $H^+ + A^-$, see: Lias, S. G.; Bartmess, J. E.; Liebman, J. F.; Holmes, J. L.; Levin, R. D.; Mallard, W. G. *Gas-Phase Ion and Neutral Thermochemistry, J. Phys. Chem. Ref. Data*; American Chemical Society; New York, 1988; Vol. 17, Suppl. No. 1.

(40) Yamataka, H.; Mustanir; Mishima, M. *J. Am. Chem. Soc.* **1999**, *121*, 10223−10224.

(41) Cumming, J. B.; Kebarle, P. *Can. J. Chem.* **1978**, *56*, 1.

(42) Bartmess, J. E.; Scott, J. A.; McIver, R. T., Jr. *J. Am. Chem. Soc.* **1979**, *101*, 6047.

(43) Blondel, C.; Cacciani, P.; Delsart, C.; Trainham, R. *Phys. Rev. A* **1989**, *40*, 3698.
(44) *NIST Standard Reference Database*, Number 69, February 2000 Release; Mallard, W. G., Ed.; http://webbook.nist.gov/chemistry.
(45) Okada, S.; Abe, Y.; Yamabe, S. *J. Phys. Chem.* **1995**, *99*, 16877.
(46) Bierbaum, V. M.; Grabowski, J. J.; DePuy, C. H. *J. Phys. Chem.* **1984**, *88*, 1389.
(47) Schroder, D.; Schalley, C. A.; Harvey, J. N.; Schwarz, H. *Int. J. Mass Spectrom.* **1999**, *185/186/187*, 25.
(48) Knobel, Yu. K.; Miroshnichenko, E. A.; Lebedev, Yu. *Izv. Akad. Nauk SSSR, Ser. Khim.* **1971**, *20*, 425.
(49) McKee, M. L. *J. Am. Chem. Soc.* **1986**, *108*, 5784.
(50) (a) Shapley, W. A.; Bacskay, G. B. *J. Phys. Chem. A* **1999**, *103*, 4505. (b) Shapley, W. A.; Bacskay, G. B. *Theor. Chim. Acta* **1998**, *100*, 212.
(51) O'Bannon, P. E.; Sultzle, D.; Dailey, W. P.; Schwarz, H.*J. Am. Chem. Soc.* **1992**, *114*, 344.
(52) Grandinetti, F.; Hrusak, J.; Schroder, D.; Schwarz, H. *J. Phys. Chem.* **1992**, *96*, 2100.